Geophysical Research Letters

RESEARCH LETTER
10.1029/2024GL110887

Distribution Characteristics and Dynamics of Marine Hydrogen in the Eastern Indian Ocean

Yu-Cheng Jiang[1,2], Gao-Bin Xu[1,2], Feng Xu[2], Jian Wang[2], Li-Min Zhou[2], Hong-Hai Zhang[1,2], and Zhao-Hui Chen[3]

[1]Frontiers Science Center for Deep Ocean Multispheres and Earth System, and Key Laboratory of Marine Chemistry Theory and Technology, Ministry of Education, Qingdao, China, [2]College of Chemistry and Chemical Engineering, Ocean University of China, Qingdao, China, [3]Key Laboratory of Physical Oceanography, Ministry of Education, Ocean University, Qingdao, China

Abstract The ocean serves as a significant contributor of atmospheric Hydrogen (H_2) with indirect greenhouse effects. However, uncertainties persist regarding internal production and consumption processes of marine H_2, as well as controlling factors. Our study examined the spatial distribution and source-sink dynamics of marine H_2 in the Eastern Indian Ocean. H_2 concentrations in surface seawater exhibited a range of 2.95–21.96 nmol L^{-1}. High concentrations of H_2 were observed in the anoxic water in the Bay of Bengal. Rates of H_2 photo-production and microbial consumption in surface seawater ranged from 1.80 to 17.78 nmol L^{-1} h^{-1} and 1.02–9.18 nmol L^{-1} h^{-1}, respectively. When considering the entire mixed layer, photo-production contribute to approximately 31%–43% of the total H_2 removal, with cyanobacteria potentially serving as another source in the mixed layer. Compared with the sea-to-air exchange, microbial consumption was the primary removal pathway of H_2 in seawater.

Plain Language Summary Atmospheric hydrogen (H_2) can influence the environment and climate by consuming hydroxyl radicals (OH·) and indirectly raising greenhouse gas concentrations. Although the ocean serves as a significant source of atmospheric H_2, the biogeochemical processes governing its presence in seawater remain poorly understood. The Eastern Indian Ocean, characterized by a substantial inflow of freshwater, exerts a distinct impact on the local ecosystem. We conducted a field investigation in the Eastern Indian Ocean to clarify the sources, sinks, and controlling factors of H_2, including the Bay of Bengal with relatively higher primary productivity and the Eastern Equatorial Indian Ocean with low primary productivity, respectively. Our study involved the quantitative assessment of H_2 photo-production, microbial consumption, and sea-to-air exchange in seawater, along with the calculation of the H_2 budget in the mixed layer. This investigation enhances our understanding of H_2 cycling processes in seawater and contributes to the assessment of H_2 emissions from the ocean and their impact on the atmospheric budget.

Yu-Cheng Jiang and Gao-Bin Xu contributed equally to this study.

Key Points:

- The distribution of H_2 was significantly affected by river input in the Eastern Indian Ocean
- Photo-production was an important source of H_2 in the mixed layer
- Microbial consumption was the primary sink for H_2 in the mixed layer

Supporting Information:

Supporting Information may be found in the online version of this article.

Correspondence to:

H.-H. Zhang,
honghaizhang@ouc.edu.cn

Citation:

Jiang, Y.-C., Xu, G.-B., Xu, F., Wang, J., Zhou, L.-M., Zhang, H.-H., & Chen, Z.-H. (2024). Distribution characteristics and dynamics of marine Hydrogen in the Eastern Indian Ocean. *Geophysical Research Letters*, *51*, e2024GL110887. https://doi.org/10.1029/2024GL110887

Received 18 JUN 2024
Accepted 18 OCT 2024

1. Introduction

Molecular hydrogen (H_2) is the second most abundant reducing gas in the troposphere after methane (Ehhalt & Prather, 2001). Its residence time is estimated between 1.4 and 2.3 years (Rhee et al., 2006; Sanderson et al., 2003; Xiao et al., 2007). H_2 reacts with hydroxyl radicals (OH·), indirectly increasing the concentrations of CH_4 and the other greenhouse gases (Ehhalt & Rohrer, 2009; Popa et al., 2015; Schultz et al., 2003; Warwick et al., 2004). Consequently, H_2 is deemed as an indirect greenhouse gas influencing global climate. In general, the sources of H_2 in the atmosphere include the emissions from fossil fuel use, biomass burning, photochemical oxidation of volatile organic compounds, nitrogen (N_2) fixation, and ocean emission (Ehhalt & Rohrer, 2009). The ocean contributes to the global H_2 budget, estimated between 2 and 6 Tg yr^{-1}, with notable uncertainties (Ehhalt & Rohrer, 2009; Hauglustaine & Ehhalt, 2002; Novelli et al., 1999; Pieterse et al., 2013). These uncertainties arise from extrapolations based on limited data regarding the entire oceanic contribution.

The concentration of H_2 is typically supersaturated in surface seawater (Herr & Barger, 1978; Moore et al., 2009; Punshon et al., 2007; Schropp et al., 1987). The N_2 fixation has been widely recognized to be an important source of H_2 (Moore et al., 2009; Scranton, 1984). In this process, H_2 is produced as a specific byproduct in the following reaction:

$$N_2 + 8H^+ + 8e^- + 16ATP \rightarrow 2NH_3 + H_2 + 16ADP + 16P_i\infty$$

Marine N_2 fixation is primarily driven by cyanobacteria in warm and oligotrophic seawater (Mahaffey et al., 2005; Shiozaki et al., 2010). Biological H_2 production mediated by anaerobic bacteria in low-oxygen areas has been considered a possible process (Herr et al., 1984; Schropp et al., 1987). Moreover, laboratory simulation experiments have shown that abiotic photo-production from chromophoric dissolved organic matter (CDOM) and low molecular weight organic matter such as acetaldehyde could lead to H_2 production (Punshon & Moore, 2008). However, there is still a lack of in-situ data regarding the photo-production of H_2 in seawater. The microbial consumption of H_2 is thermodynamically favorable and indeed occurs (Herr et al., 1981, 1984). Additionally, the high saturation of H_2 in surface seawater results in a net flux from the ocean to the atmosphere (Punshon et al., 2007).

The Eastern Indian Ocean is a semi-open ocean, and its marine ecosystem is influenced by a variety of land-based inputs due to its unique geographical location. River inflow notably impacts the ecosystem in the Eastern Indian Ocean, especially in the Bay of Bengal (Ghosh et al., 2024; Shetye et al., 1991). Many rivers in the Asian continent, such as the Ganges and Brahmaputra, feed large amounts of fresh water, nutrients and organic matter into the Bay of Bengal. These inputs markedly affect the bay's physical, chemical, and biological processes (Sengupta et al., 2006), which potentially influence the H_2 source and sink processes. For example, the latest research showed the concentration of microplastics would influence the production of H_2, while the Ganges is an important source of microplastics in the bay (Alam et al., 2023; Wei et al., 2022), which could enhance the concentration of H_2 in seawater. Additionally, the substantial freshwater input leads to strong stratification in the near-surface layer that inhibits vertical mixing, creating a sharp and intense oxygen minimum zone (Rao et al., 2016). The exchange of gases between the sea and air in the Eastern Indian Ocean is highly active, facilitated by the monsoon winds and elevated surface seawater temperatures. This may have a great impact on the atmospheric H_2 budget. In this study, we investigated the distribution characteristics and controlling factors of H_2 and calculated the sea-to-air flux of H_2 during autumn. Additionally, we conducted in-situ irradiation and incubation experiments to examine the photo-production and microbial consumption of H_2. These observations aim to provide important data support for the global scale emission of H_2 from the ocean and understand the regional characteristics and biogeochemical cycling process of H_2.

2. Methods

2.1. Voyage and Sampling

Our measurements were conducted on board the R/V "*Shiyan 3*" in the Eastern Indian Ocean from 27 September to 6 November 2020. The study area and detailed sampling stations are shown in Figure 1. The seawater samples of H_2 were collected from 64 stations by using 12-L volume Niskin bottles installed in a Seabird 911 conductivity-temperature-depth (CTD) rosette, from which seawater salinity and temperature were also recorded. Atmospheric H_2 samples were collected on the deck about 10 m above the sea level. To avoid pollution caused by ship sailing, all atmospheric samples were collected windward with a 10 mL airtight syringe while the ship was sailing. Samples for other environment parameters (chlorophyll-*a*, dissolved organic carbon [DOC], CDOM, nutrients, and cyanobacteria) were treated onboard for storage and brought back to the laboratory for analysis. The sampling and analytical methods are described Text S1–S3 in Supporting Information S1. In addition to sampling, in-suit incubation experiments were conducted at 11 stations.

2.2. Analysis Method of H_2

In this study, all H_2 samples were measured onboard by Trace 3000R reduced gas detector (Ametek, USA). Before analysis, the instrument was calibrated using the H_2 standard gas with a mixing ratio of 500 ppbv, supplied by the State Center for Standard Matter (China). The calibration was repeated every day. The measurement of H_2 in seawater was conducted using the headspace equilibrium method (Xie et al., 2002). A 50 ml bottle was filled with a seawater sample collected in the field, sealed, and then the seawater sample was replaced with 8 mL of high purity N_2 (purity >99.99999%) using a gas-tight syringe. The treated sample was shaken at 300 r min^{-1} for 5 min to ensure that the headspace in the bottle was in gas-liquid equilibrium; 6 mL of the equilibrium gas was extracted using a gas-tight syringe and injected through PTFE hydrophobic filter membrane into the instrument for determination. The measured value was converted to obtain the concentration of H_2 in seawater. The specific

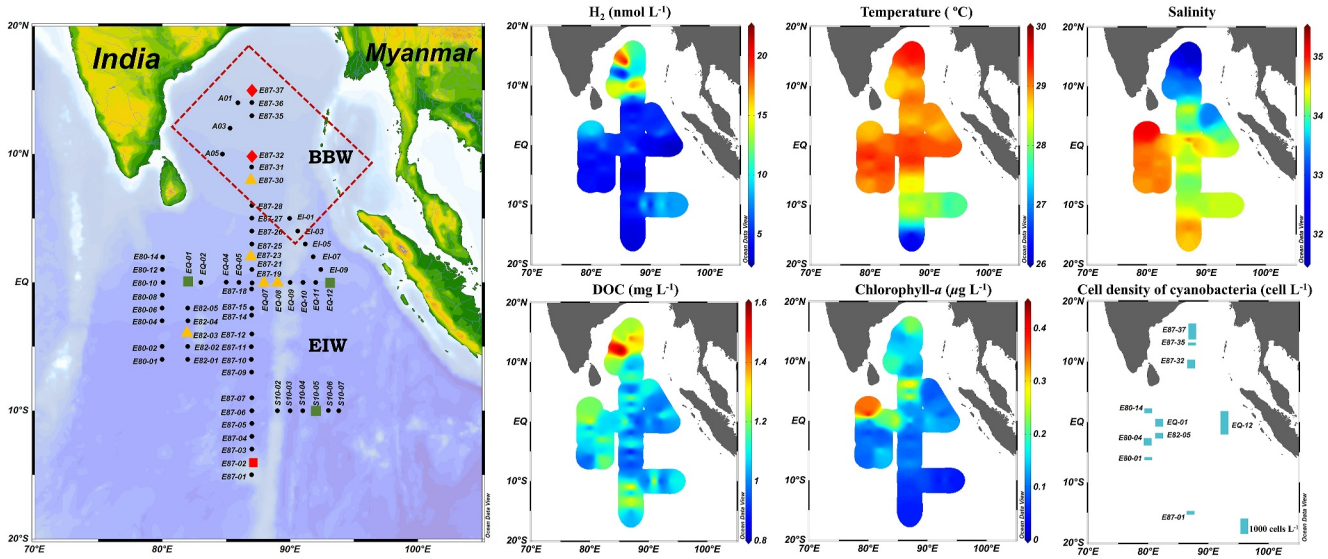

Figure 1. Location of the sampling stations (red rhombus: Stations for microbial consumption and irradiation experiments; yellow triangle: Stations for irradiation experiments; green square: Stations for microbial consumption; BBW: Bay of Bengal water; EIW: Eastern equatorial Indian Ocean water) and Horizontal distribution of temperature, salinity, H_2, DOC, chlorophyll-*a* and cyanobacteria (pico-) in the surface seawater (about 5 m).

calculation formulas are shown Text S4 in Supporting Information S1. The detection limit was 0.02 nmol L^{-1} with a relative standard deviation of less than 4.4%.

2.3. Incubation Experiments

2.3.1. Photo-Production

An in-situ irradiation experiment was selectively conducted to determine the photochemical production rates of H_2 and assess the influence of different wavelengths on this process. To avoid the influences of algae, microorganisms, and particles, seawater samples were filtered twice directly into pre-cleaned bottles through 0.22 μm polyethersulfone filters that were thoroughly rinsed with sample water (Park et al., 2021). Filtered samples were then transferred into 150 ml quartz tubes with Teflon stoppers for subsequent spectral treatments: (a) quartz tubes (full-spectrum solar radiation). (b) one layer of UF3 Plexiglas-wrapped quartz tubes (attenuating all UV and transmitting most of the visible light). (c) three layers of aluminum foil-wrapped quartz tubes (dark). The UV radiation results were obtained by subtracting the results of the PAR light from the results of the full-spectrum solar radiation. All quartz tubes were exposed to solar radiation in an incubator equipped with circulation equipment to maintain the in-situ temperature of the seawater samples. All samples were cultured for a duration of 6 hr, after which 50 mL aliquots were taken to determine the H_2 concentration. Measurements were taken at half-hourly intervals using a UV-Vis spectroradiometer (OL 756, Gooch and Housego, UK), with the incident photon flux density being recorded.

We assessed and integrated the photo-production process of H_2 resulting from UV and PAR across the water column. The light intensity for a specific type of radiation, denoted as *X*, at a depth of *Z* (PFD [X, Z]), can be derived from the surface light intensity (PFD [X, 0]) by exponentially attenuating it with depth, as prescribed by the Beer-Lambert equation:

$$\mathrm{PFD}\,[X,Z] = \mathrm{PFD}\,[X,0] \times e^{-kxZ}$$

Light attenuation underwater is primarily influenced by four main factors: water itself, CDOM, chlorophyll-*a,* and particles. The concentration of particular matter is generally low in the open ocean, and thus particles was omitted from our calculation (Pérez et al., 2016). Numerous studies have demonstrated a strong correlation between the UV attenuation coefficient and CDOM (Johannessen et al., 2003; Para et al., 2013), with CDOM recognized as the primary contributor to UV attenuation in the ocean (Pérez et al., 2016). Therefore, in our study, the UV attenuation coefficient (k_X, m^{-1}) is approximated as the sum of the absorption coefficient of pure water

(Buiteveld et al., 1994; Pope & Fry, 1997) and the CDOM absorption coefficient at the corresponding wavelength (a_W [X] and a_{CDOM} [X], m^{-1}):

$$k_{uv} = a_W\,(UV) + a_{CDOM}\,(UV)$$

The attenuation of solar radiation by phytoplankton mainly affects PAR. The attenuation coefficient of phytoplankton can be expressed by the concentration of chlorophyll-*a* ([Chl], mg L^{-1}), and the formula is as follows (Kloster et al., 2006):

$$k_{phy} = 0.03 \times [Chl]$$

The attenuation coefficient of PAR waveband (k_{PAR} m^{-1}) can be expressed as:

$$k_{PAR} = a_W(PAR) + a_{CDOM}(PAR) + k_{phy}$$

Combined with the attenuation formula of solar radiation, the photo-production rate at *X* waveband of depth *Z* (*K* [X, Z]) can be expressed as:

$$K(X,Z) = K(X,0) \times PFD(X,Z) \,/\, PFD(X,0) = K(X,0) \times e^{-kxZ}$$

The mixed layer depth was defined as the depth at which the density was 0.03 kg m^{-3} lower than surface water (to the reference depth of 10 dbar) (de Boyer Montégut et al., 2004).

2.3.2. Microbial Consumption

Surface seawater was collected to investigate the microbial consumption rates of H_2. Seawater samples were incubated on board in 500 ml airtight glass syringes onboard. Urea was added to the syringes to achieve a final concentration of 10 mmol L^{-1}, which served to inhibit the N_2 fixation (Rawson, 1985). As for the control group, the water samples underwent repeated filtration through 0.22 μm polyethersulfone filters for twice. Subsequently, all samples were placed in a lightproof incubator to prevent photoreaction and the in-situ surface seawater temperature was maintained by circulating surface seawater. After a 6 hr incubation, the concentration of H_2 was determined in both the experimental group and control group to calculate the microbial consumption rate of H_2.

2.4. Sea-To-Air Flux of H_2

The instantaneous sea-to-air flux (*F*) of H_2 was calculated by the two-layer model (Liss & Merlivat, 1986):

$$F = k\left([H_2]_{surf} - [H_2]_{eq}\right)$$

where *F* is the flux (nmol·m^{-2}·hr^{-1}); *k* is the sea-to-air exchange velocity (m·s^{-1}); $[H_2]_{surf}$ and $[H_2]_{eq}$ represent the initial concentration of H_2 in surface seawater and the concentration of H_2 in seawater when atmospheric H_2 is at equilibrium with the seawater. Detailed calculation formulas are provided Text S4 in Supporting Information S1.

3. Results and Discussion

3.1. Oceanographic Background

Vertical profiles of temperature, salinity, chlorophyll-*a*, dissolved oxygen, DOC, and nutrients at a depth of 0–200 m along 87°E transect in the Eastern Indian Ocean are illustrated in Figure S1 in Supporting Information S1. The substantial influx of fresh water into the Bay of Bengal has led to a wide range of surface salinity (31.79–35.18) across the study area, limiting the transport of oxygen from mixed layer to subsurface seawater which resulted in the formation of low oxygen zones. It suggested that the study area exhibited different marine environments. Through K-means cluster analysis of the surface salinity (Table S1 in Supporting Information S1), the area was partitioned into the Bay of Bengal water (BBW) and the Eastern Equatorial Indian Ocean Water (EIW) to explore the distribution characteristics of and biogeochemical processes of H_2 in different environments. The concentration of DOC in surface seawater of the two regions showed a significant difference (t = 2.095,

$p < 0.005$). Notably, the two highest concentrations of DOC in surface seawater both appeared in the Bay of Bengal (A03: 1.589 mg L^{-1}; E87-36: 1.466 mg L^{-1}). This was due to the abundant organic matter entering the Bay of Bengal along with fresh water. The other environment parameters of two regions are shown in Table S2 in Supporting Information S1.

3.2. Distributions and Controlling Factors of H_2

3.2.1. Horizontal Distribution of H_2 in Seawater

Horizontal distribution of temperature, salinity, H_2, chlorophyll-*a,* DOC and cyanobacteria (pico-) are shown in Figure 1. The average concentrations of H_2 in surface seawater were 10.66 ± 5.67 (3.81–21.96) nmol L^{-1} and 4.98 ± 1.91 (2.75–9.98) nmol L^{-1} in BBW and EIW, respectively. The concentration of H_2 in BBW significantly exceeded that in EIW ($t = 3.133$, $p < 0.001$). We compared the concentrations of H_2, chlorophyll-*a* and cell density of cyanobacteria in the surface seawater and found no correlation between them. However, a relationship was observed between the H_2 concentration and the cell density of *Trichodesmium* sp ($r = 0.833$, $n = 7$, $p < 0.05$, Table S3 in Supporting Information S1). Since H_2 is a byproduct of N_2 fixation while *Trichodesmium* is the important undertaker (Capone et al., 1997; Scranton, 1984), it suggests that N_2 fixation play a significant role in H_2 production. In addition, high concentrations of H_2 were observed in low salinity stations of the Bay of Bengal, exhibiting a significant negative correlation with salinity ($r = -0.547$, $n = 64$, $p < 0.01$, Table S4 in Supporting Information S1). This might be attributed to the river input, which provided large amounts of freshwater, nutrients, and organic matter, influencing the biogeochemical processes of H_2 in the Eastern Indian Ocean. To further explore the cause of high H_2 value in the BBW, the production and loss processes of marine H_2 have been conducted and will be discussed in the following sections.

3.2.2. Distribution of H_2 in Anoxic Seawater

The vertical profiles at most stations in EIW presented that the highest H_2 concentration occurred within the upper 50 m, with a rapid decrease below this depth and fluctuated slightly (Figure S1 in Supporting Information S1). Conversely, a distinct vertical distribution trend was observed in BBW, where higher H_2 values were consistently found in anoxic water layers (DO < 2.00 mg L^{-1}). For instance, concentrations of H_2 measured at a depth of 150 m at E87-37 station (20.84 nmol L^{-1}) and A03 (12.20 nmol L^{-1}) were 1.85 and 3.84 times higher than those in the surface seawater, respectively. Schropp et al. (1987) conducted a nutrient enrichment experiment on anoxic seawater, revealing elevated anaerobic production rates of H_2. The abundance of nutrients in the anoxic water of the Bay of Bengal (seen in Figure S2 in Supporting Information S1) likely promoted the growth of anaerobic bacteria, thereby facilitating the release of H_2.

3.3. Photo-Production of H_2

3.3.1. Photo-Production of H_2 in the Surface Seawater

The rates of H_2 photo-production driven by UV and PAR in surface seawater, along with cumulative solar radiation photon fluxes, are depicted in Figure 2. The photo-production under full-spectrum radiation (K_{photo}) was 13.31 ± 4.28 (7.53–17.77) nmol L^{-1} h^{-1} and 2.12 ± 1.47 (1.80–5.78) in the BBW and EIW. Dark control experiments did not yield significant H_2 production. The average cumulative solar radiation photon fluxes during irradiation experiments were similar between BBW (12.59 ± 3.51 *E* m^{-2}) and EIW (12.55 ± 2.97 *E* m^{-2}). Variances in H_2 photo-production rates between the two regions can be ascribed to differences in physicochemical properties, CDOM contents and compositions, and photosensitizer (nitrate) levels (Mack & Bolton, 1999). The absorption coefficient at 280 nm is used as a proxy to estimate CDOM concentration (Andrew et al., 2013). Our experiment results demonstrated a correlation between H_2 photo-production rate and both CDOM ($r = 0.820$, $n = 8$, $p < 0.05$) and nitrate ($r = 0.846$, $n = 8$, $p < 0.01$), respectively. The *a*CDOM (280) in the BBW (0.68 ± 0.07 m^{-1}) was higher than that in the EIW (0.53 ± 0.05 m^{-1}) and the nitrate concentration in surface seawater was also higher in BBW (0.033 ± 0.028 μmol L^{-1}) compared to EIW (0.024 ± 0.021 μmol L^{-1}). The elevated levels of CDOM and photosensitizer in BBW contributed to higher H2 photo-production rates.

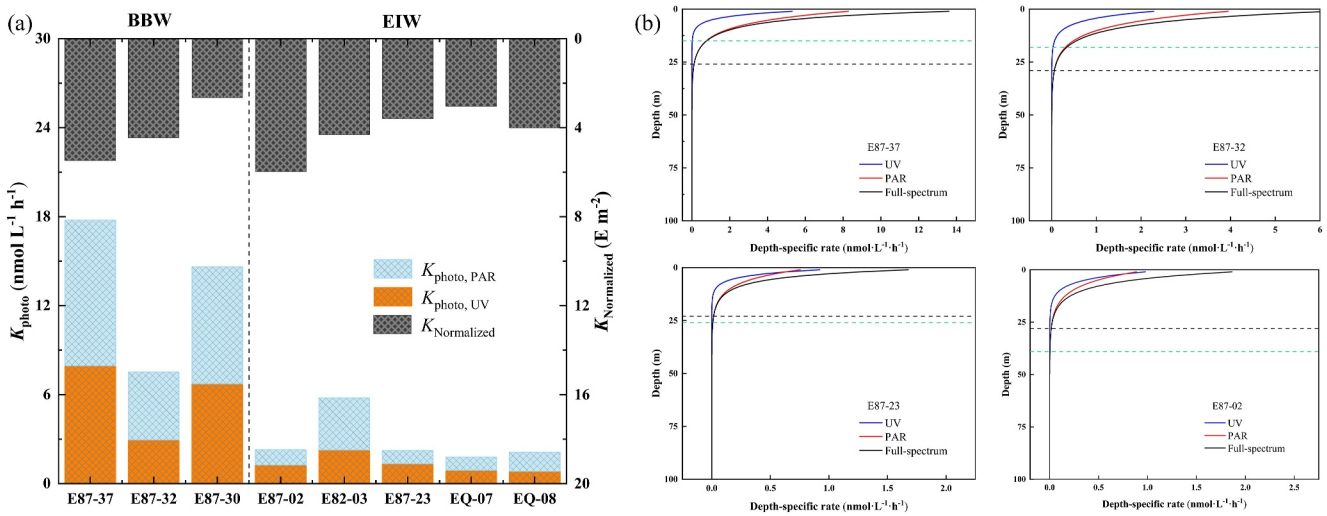

Figure 2. (a) H_2 photo-production rates (K_{photo}) in ultraviolet radiation (UV) and photosynthetically active radiation (PAR) of surface seawater at each station with solar radiation photon fluxes ($K_{normalized}$) (the dotted line shows the boundary between the Bay of Bengal Water [BBW] and the Eastern Indian Ocean water [EIW]). (b) Modeled depth-specific (nmol L^{-1} h^{-1}) of ultraviolet radiation (UV) and photosynthetically active radiation (PAR) mediated H_2 photo-production in the entire water column (depth-specific rates were integrated across the specified water column depth to obtain depth-integrated rates; the green and black dotted line represents the mixed layer depth and effective photo-production activity depth, respectively).

3.3.2. Effects of Radiation Quality on Photo-Production

The average rates of UV (K_{UV}) and PAR (K_{PAR}) in BBW were 5.87 ± 2.13 and 7.44 ± 2.16 nmol L^{-1} h^{-1}, and those in EIW were 1.32 ± 0.52 and 1.53 ± 1.00 nmol L^{-1}, respectively. The average integral photo fluxes for UV and PAR during the experiments were calculated to be 0.46 ± 0.02 *E* m^{-2}, 12.2 ± 3.50 *E* m^{-2} in the BBW, and 0.96 ± 0.38 *E* m^{-2}, 11.8 ± 2.73 *E* m^{-2} in EIW, respectively. Despite UV radiation accounting for less than 10% of the total solar radiation, it contributed on average 43.2% ± 3.0% and 46.3% ± 8.4% of the total H_2 photo-production in BBW and EIW, respectively. In addition, we gave a normalized H_2 photo-production ratio, for UV: PAR of 45: 1 and 19: 1 in the BBW and EIW, respectively. It indicated that the UV efficiency of surface seawater in the BBW was higher than EIW. The ratio of the spectral slope (SR) of the shorter waveband (275–295 nm) to that of the longer waveband (350–400 nm) distinguished the origin of CDOM; smaller SR value indicated a higher proportion of terrestrial CDOM and vice versa for marine source. As shown in Table S5 in Supporting Information S1, the S_R in the BBW (1.617–1.824) was smaller than that in EIW (1.880–3.345), which indicated that the terrestrial CDOM was more prone to photochemical reaction and had a higher efficiency for H_2 photo-production.

3.3.3. Modeled Photo-Production Throughout the Mixed Layer

To scale the experiment results to the water column, we simulated the H_2 photo-production rates in the entire upper water for all irradiation stations (Figure 2b and Figure S3 in Supporting Information S1). Since the mixed layer is the depth horizon that regulates sea-to-air exchange, the following analysis focused on the photo-production within the mixed layer. We integrated the photo-production rates of UV and PAR within the depth to facilitate a more intuitive comparison of their contributions to H_2 photo-production in the mixed layer. To roughly assess the influence of H_2 photo-production in water column, an effective photo-production depth was defined as the depth at which solar radiation attenuates to 1% of the sea surface. If the depth of the mixed layer was shallower than the effective photo-production layer, the depth-integrated rate was calculated within the mixed layer depth. Otherwise, it was calculated within the effective photo-production layer depth. The average depth-integrated rate of UV and PAR in the mixed layer were 8.73 ± 5.74 (2.66–18.36) μmol m^{-2} h^{-1} and 19.3 ± 14.1 (4.77–41.1) μmol m^{-2} h^{-1}, respectively, with average contributions to H_2 photo-production of approximately 31% and 69%, respectively. Compared with the process of H_2 photo-production in surface seawater, PAR emerged as the dominant driver of photo-production in the mixed layer.

3.4. Microbial Consumption of H_2

The microbial consumption rates of H_2 (K_{micro}) were calculated to be 6.70 ± 2.48 (4.22–9.18) and 1.39 ± 1.94 (1.02–1.91) nmol L^{-1} h^{-1} in the BBW and EIW. A positive correlation between microbial consumption rate and H_2 concentration was observed ($r = 0.827$, $n = 6$, $p < 0.05$) across the entire study area, indicating that higher H_2 concentrations were associated with faster microbial consumption rates. The consumption rates in EIW were comparable to those reported by Scranton (1984) (1.25–1.95 nmol L^{-1} h^{-1}), while the consumption rates in BBW were generally higher. It could be attributed to the abundance of bacteria in the Bay of Bengal. A previous study found a strong positive correlation between bacterial abundance and chlorophyll-*a* concentration (Bird & Kalff, 1984). The average concentration of chlorophyll-*a* of microbial consumption stations in the BBW (0.20 ± 0.04 μg L^{-1}) was higher than that in the EIW (0.11 ± 0.07 μg L^{-1}) (despite the lack of statistical significance), indicating that bacteria in the BBW possessed higher activity and more efficient removal of H_2.

3.5. Sea-To-Air Flux

The average instantaneous sea-to-air flux of H_2 was 7.29 ± 6.04 (0.49–26.0) μmol m^{-2} d^{-1}. The Eastern Indian Ocean was a net source of atmospheric H_2. Our flux estimates were higher than previous investigations in the Northern Atlantic Ocean (3.04 μmol m^{-2} d^{-1}) and the Southern Atlantic Ocean (2.10 μmol m^{-2} d^{-1}), which could be attributed to the higher concentrations of H_2 (the Northern Atlantic Ocean: 0.18–3.26 nmol L^{-1}, the Southern Atlantic Ocean:0.40–1.40 nmol L^{-1}) (Herr & Barger, 1978; Herr et al., 1984).

The sea-to-air flux of H_2 did not show a statistical difference between the two regions. It could be attributed to the effect of wind speeds and temperature of seawater on the sea-to-air exchange. A sensitivity analysis was conducted to evaluate the impact of these factors on the sea-to-air exchange, as shown in Figure S4a in Supporting Information S1. The results indicated that wind speed, seawater temperature, and H_2 concentration all affected the sea-to-air flux. Among these factors, wind speed exerted the most significant influence, followed by H_2 concentrations. A strong correlation was observed between wind speed and flux, with a 55% variation in H_2 flux (Figure S4b in Supporting Information S1). The higher wind speeds in the EIW (8.99 m s^{-1} vs. 6.58 m s^{-1} in the BBW) promoted this process. Although the concentration of H_2 in the BBW was significantly higher than that in EIW, it was insufficient to offset the effect of wind speed, resulting in comparable sea-to-air fluxes between the two regions.

3.6. Budget of H_2 in the Mixed Layer

We developed a budget model based on our research (Figure 3), to detail the source-sink dynamics of marine H_2 within the mixed layer. This model elucidated the biogeochemical process and rates of H_2. Since the H_2 photo-production rate varied significantly with depth, the average photo-production rates of the mixed layer were calculated as the quotient between depth-integrated rate across the mixed layer and the depth of the mixed layer. Turnover times for each removal pathway were calculated using the initial H_2 concentrations divided by their corresponding rates (Table S6 in Supporting Information S1).

Rates of microbial consumption and sea-to-air exchange within the mixed layer were 6.70 ± 2.48 and 0.0176 ± 0.001 nmol L^{-1} h^{-1} in BBW, and those in EIW were 1.39 ± 0.33 and 0.0067 ± 0.004 nmol L^{-1} h^{-1}, respectively. It indicated that the majority of H_2 participated in the biogeochemical process, and only a small portion was emitted to the atmosphere. The total turnover times of H_2 were 0.10 ± 0.02 and 0.13 ± 0.05 days in BBW and EIW, respectively, suggesting the H_2 turnover in the Eastern Indian Ocean could be highly dynamic. The average rate of photo-production in the mixed layer in BBW (2.87 ± 0.86 nmol L^{-3} h^{-1}) was higher than that in EIW (0.44 ± 0.27 nmol L^{-3} h^{-1}), which could explain about 43% and 31% of the total removal of H_2 in the BBW and EIW, respectively. This high level of photosensitizer and CDOM resulted in a relatively higher contribution of photo-production in the mixed layer of BBW. However, it was evident that the photo-production could not maintain the turnover of H_2. Moore et al. (2009) observed a correlation between N_2 fixation rate (μmol N m^{-3} d^{-1}) and H_2 concentration (nmol L^{-1}) in the Pacific Ocean (N_2 fixation = 1.73 [H_2] – 0.15, $r = 0.98$). Previous studies found that the N_2 fixation rate in the Eastern Indian Ocean is not lower than that in the Pacific Ocean (Shao et al., 2023). In addition, Price et al. (2007) estimated the N_2 fixation contribute at least 55% to total production of H_2 in the ocean, which suggested that the gap between sources and sinks of H_2 could be attributed to the N_2 fixation.

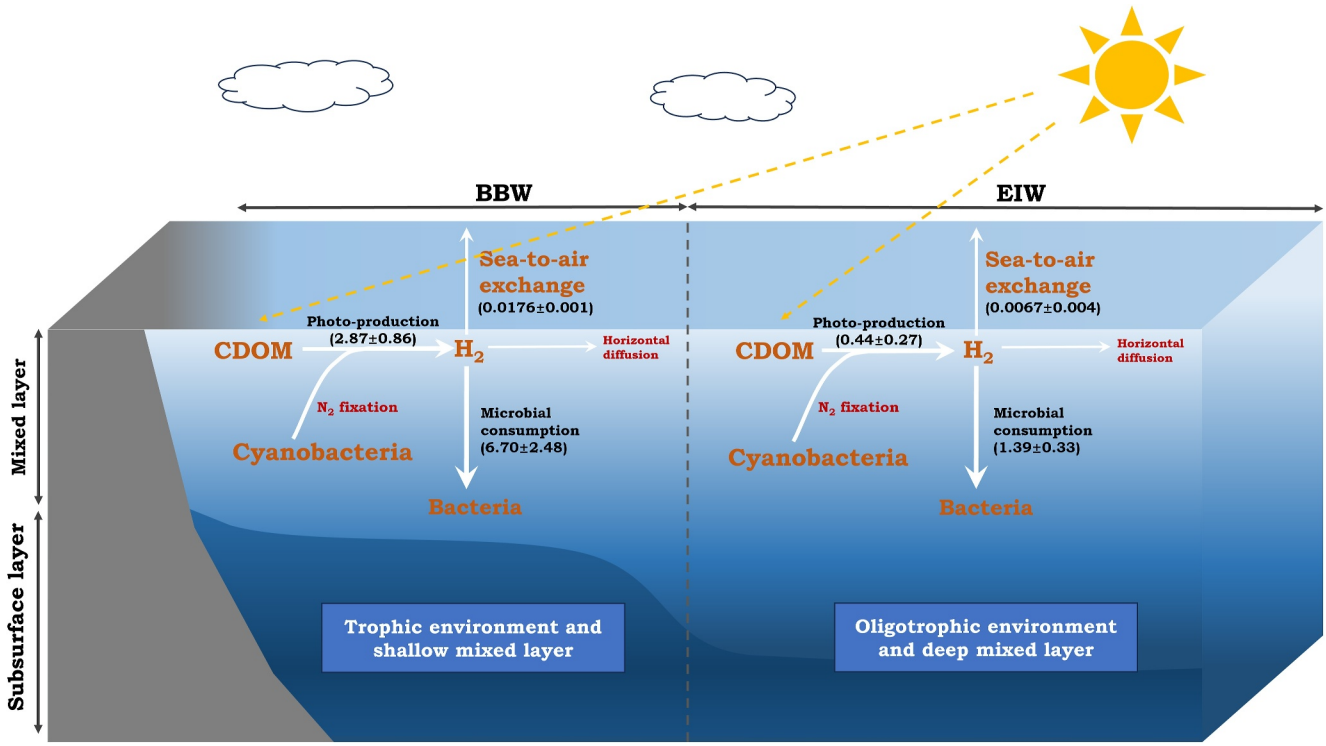

Figure 3. Source-sink budget models for the H_2 within the mixed layer in the BBW and EIW region of the Eastern Indian Ocean (The red letters are potential source and sink of hydrogen). The numerical values in the figure indicate that the mean rates (standard deviation) of source and sink within the mixed layer in the study survey are expressed in nmol L^{-1} h^{-1}.

4. Summary

We conducted a systematic investigation in the Eastern Indian Ocean to get new insight into the occurrence and cycle of H_2 and assess the H_2 budget in the mixed layer for the first time. Elvated concentration of H_2 was primarily detected in region impacted by river input. In-situ incubation experiment revealed that photo-production rates of H_2 in the surface seawater were related to the CDOM and photosensitizer. The region with a high proportion of terrestrial CDOM had higher efficiencies of photo-production. The photo-production efficiency of the UV waveband was much higher than that of PAR, though the UV radiation only accounted for a fraction of the total solar radiation, it contributed more than 40% of the H_2 photo-production. Compared with the surface seawater, the proportion of H_2 photo-production in the UV waveband in the mixed layer was reduced, and the PAR was the dominant driver of photo-production. Microbial consumption was the main way of H_2 removal instead of sea-to-air exchange. Considering the budget in the mixed layer, the photo-production could not maintain the total removal of H_2. N_2 fixation could be another important source of H_2. These results clarify the in-situ concentrations and relative importance of different sources and sinks of the Eastern Indian Ocean, which improve our understanding of the cycling of H_2 in marine.

Data Availability Statement

Data presented in this paper are publicly available at Figshare via Jiang (2024).

Acknowledgments
We thank the captain and crews of the R/V "Shiyan 3" for their assistance and cooperation during the investigation. This work was financially supported by the National Natural Science Foundation of China (Grant 42276042, 41876082 and 42225601), the Laoshan Laboratory (Grant LSKJ202201701), and the Fundamental Research Funds for the Central Universities (Grant 202372001 and 202072001).

References

Alam, M. J., Shammi, M., & Tareq, S. M. (2023). Distribution of microplastics in shoreline water and sediment of the Ganges river basin to meghna estuary in Bangladesh. *Ecotoxicology and Environmental Safety*, *266*, 115537. https://doi.org/10.1016/j.ecoenv.2023.115537

Andrew, A. A., Del Vecchio, R., Subramaniam, A., & Blough, N. V. (2013). Chromophoric dissolved organic matter (CDOM) in the Equatorial Atlantic Ocean: Optical properties and their relation to CDOM structure and source. *Marine Chemistry*, *148*, 33–43. https://doi.org/10.1016/j.marchem.2012.11.001

Bird, D. F., & Kalff, J. (1984). Empirical relationships between bacterial abundance and chlorophyll concentration in fresh and marine waters. *Canadian Journal of Fisheries and Aquatic Sciences*, *41*(7), 1015–1023. https://doi.org/10.1139/f84-118

Buiteveld, H., Hakvoort, J., & Donze, M. (1994). Optical properties of pure water. *Ocean Optics*, *2258*(6), 368–373. https://doi.org/10.1117/12.190060

Capone, D. G., Zehr, J. P., Paerl, H. W., Bergman, B., & Carpenter, E. J. (1997). Trichodesmium, a globally significant marine cyanobacterium. *Science*, *276*(5316), 1221–1229. https://doi.org/10.1126/science.276.5316.1221

de Boyer Montégut, C., Madec, G., Fischer, A. S., Lazar, A., & Iudicone, D. (2004). Mixed layer depth over the global ocean: An examination of profile data and a profile-based climatology. *Journal of Geophysical Research*, *109*(12), 1–20. https://doi.org/10.1029/2004JC002378

Ehhalt, D., & Prather, M. (2001). Atmospheric chemistry and greenhouse gases. *Climate Change 2001: The Scientific Basis*, 239–287. https://hal.science/hal-03333922/

Ehhalt, D. H., & Rohrer, F. (2009). The tropospheric cycle of H2: A critical review. *Tellus Series B Chemical and Physical Meteorology*, *61*(3), 500–535. https://doi.org/10.1111/j.1600-0889.2009.00416.x

Ghosh, J., Chakraborty, K., Valsala, V., Bhattacharya, T., & Ghoshal, P. K. (2024). A review of the Indian ocean carbon dynamics, acidity, and productivity in a changing environment. *Progress in Oceanography*, *221*, 103210. https://doi.org/10.1016/j.pocean.2024.103210

Hauglustaine, D. A., & Ehhalt, D. H. (2002). A three-dimensional model of molecular hydrogen in the troposphere. *Journal of Geophysical Research*, *107*(17). ACH 4-1–ACH 4-16. https://doi.org/10.1029/2001JD001156

Herr, F. L., & Barger, W. R. (1978). Molecular hydrogen in the near-surface atmosphere and dissolved in waters of the tropical North Atlantic. *Journal of Geophysical Research*, *83*(C12), 6199–6205. https://doi.org/10.1029/jc083ic12p06199

Herr, F. L., Frank, E. C., Leone, G. M., & Kennicutt, M. C. (1984). Diurnal variability of dissolved molecular hydrogen in the tropical South Atlantic Ocean. *Deep-Sea Research, Part A: Oceanographic Research Papers*, *31*(1), 13–20. https://doi.org/10.1016/0198-0149(84)90069-4

Herr, F. L., Scranton, M. I., & Barger, W. R. (1981). Dissolved hydrogen in the Norwegian Sea: Mesoscale surface variability and deep-water distribution. *Deep-Sea Research, Part A: Oceanographic Research Papers*, *28*(9), 1001–1016. https://doi.org/10.1016/0198-0149(81)90014-5

Jiang, Y. C. (2024). Distribution characteristics and dynamics of marine hydrogen in the eastern Indian ocean. *Figshare*. [Dataset]. https://doi.org/10.6084/m9.figshare.26048188

Johannessen, S. C., Miller, W. L., & Cullen, J. J. (2003). Calculation of UV attenuation and colored dissolved organic matter absorption spectra from measurements of ocean color. *Journal of Geophysical Research*, *108*(9). https://doi.org/10.1029/2000jc000514

Kloster, S., Feichter, J., Maier-Reimer, E., Six, K. D., Stier, P., & Wetzel, P. (2006). DMS cycle in the marine ocean-atmosphere system - a global model study. *Biogeosciences*, *3*(1), 29–51. https://doi.org/10.5194/bg-3-29-2006

Liss, P. S., & Merlivat, L. (1986). Air-sea gas exchange rates: Introduction and synthesis. In *In the role of air-sea exchange in geochemical cycling*.

Mack, J., & Bolton, J. R. (1999). Photochemistry of nitrite and nitrate in aqueous solution: A review. *Journal of Photochemistry and Photobiology A: Chemistry*, *128*(1–3), 1–13. https://doi.org/10.1016/S1010-6030(99)00155-0

Mahaffey, C., Michaels, A. F., & Capone, D. G. (2005). The conundrum of marine N 2 fixation. *American Journal of Science*, *305*(6–8), 546–595. https://doi.org/10.2475/ajs.305.6-8.546

Moore, R. M., Punshon, S., Mahaffey, C., & Karl, D. (2009). The relationship between dissolved hydrogen and nitrogen fixation in ocean waters. *Deep-Sea Research Part I Oceanographic Research Papers*, *56*(9), 1449–1458. https://doi.org/10.1016/j.dsr.2009.04.008

Novelli, P. C., Lang, P. M., Masarie, K. A., Hurst, D. F., Myers, R., & Elkins, J. W. (1999). Molecular hydrogen in the troposphere: Global distribution and budget. *Journal of Geophysical Research*, *104*(D23), 30427–30444. https://doi.org/10.1029/1999JD900788

Para, J., Charrière, B., Matsuoka, A., Miller, W. L., Rontani, J. F., & Sempéré, R. (2013). UV/PAR radiation and DOM properties in surface coastal waters of the Canadian shelf of the Beaufort Sea during summer 2009. *Biogeosciences*, *10*(4), 2761–2774. https://doi.org/10.5194/bg-10-2761-2013

Park, J. B. K., Weaver, L., Davies-Colley, R., Stott, R., Williamson, W., Mackenzie, M., et al. (2021). Comparison of faecal indicator and viral pathogen light and dark disinfection mechanisms in wastewater treatment pond mesocosms. *Journal of Environmental Management*, *286*(October 2020), 112197. https://doi.org/10.1016/j.jenvman.2021.112197

Pérez, G. L., Galí, M., Royer, S. J., Sarmento, H., Gasol, J. M., Marrasé, C., & Simó, R. (2016). Bio-optical characterization of offshore NW mediterranean waters: CDOM contribution to the absorption budget and diffuse attenuation of downwelling irradiance. *Deep-Sea Research Part I Oceanographic Research Papers*, *114*, 111–127. https://doi.org/10.1016/j.dsr.2016.05.011

Pieterse, G., Krol, M. C., Batenburg, A. M., M. Brenninkmeijer, C. A., Popa, M. E., O'Doherty, S., et al. (2013). Reassessing the variability in atmospheric H_2 using the two-way nested TM5 model. *Journal of Geophysical Research: Atmospheres*, *118*(9), 3764–3780. https://doi.org/10.1002/jgrd.50204

Popa, M. E., Segers, A. J., Denier van der Gon, H. A. C., Krol, M. C., Visschedijk, A. J. H., Schaap, M., & Röckmann, T. (2015). Impact of a future H_2 transportation on atmospheric pollution in Europe. *Atmospheric Environment*, *113*, 208–222. https://doi.org/10.1016/j.atmosenv.2015.03.022

Pope, R. M., & Fry, E. S. (1997). Absorption spectrum (380–700 nm) of pure water II Integrating cavity measurements. *Applied Optics*, *36*(33), 8710. https://doi.org/10.1364/ao.36.008710

Price, H., Jaeglé, L., Rice, A., Quay, P., Novelli, P. C., & Gammon, R. (2007). Global budget of molecular hydrogen and its deuterium content: Constraints from ground station, cruise, and aircraft observations. *Journal of Geophysical Research*, *112*(D22), D22108. https://doi.org/10.1029/2006JD008152

Punshon, S., & Moore, R. M. (2008). Photochemical production of molecular hydrogen in lake water and coastal seawater. *Marine Chemistry*, *108*(3–4), 215–220. https://doi.org/10.1016/j.marchem.2007.11.010

Punshon, S., Moore, R. M., & Xie, H. (2007). Net loss rates and distribution of molecular hydrogen (H_2) in mid-latitude coastal waters. *Marine Chemistry*, *105*(1–2), 129–139. https://doi.org/10.1016/j.marchem.2007.01.009

Rao, G. D., Viswanadham, R., Sherin, C. K., Salisbury, J., Omand, M. M., Mahadevan, A., et al. (2016). Effects of freshwater stratification on nutrients, dissolved oxygen, and phytoplankton in the bay of bengal. *Oceanography*, *29*(2), 222–231. https://doi.org/10.5670/oceanog.2016.54

Rawson, D. M. (1985). The effects of exogenous amino acids on growth and nitrogenase activity in the cyanobacterium Anabaena cylindrica PCC 7122. *Microbiology*, *131*(10), 2549–2554. https://doi.org/10.1099/00221287-131-10-2549

Rhee, T. S., Brenninkmeijer, C. A. M., & Röckmann, T. (2006). The overwhelming role of soils in the global atmospheric hydrogen cycle. *Atmospheric Chemistry and Physics*, *6*(6), 1611–1625. https://doi.org/10.5194/acp-6-1611-2006

Sanderson, M. G., Collins, W. J., Derwent, R. G., & Johnson, C. E. (2003). Simulation of global hydrogen levels using a Lagrangian three-dimensional model. *Journal of Atmospheric Chemistry*, *46*(1), 15–28. https://doi.org/10.1023/A:1024824223232

Schropp, S. J., Scranton, M. I., & Schwarz, J. R. (1987). Dissolved hydrogen, facultatively anaerobic, hydrogen-producing bacteria, and potential hydrogen production rates in the western North Atlantic Ocean and Gulf of Mexico. *Limnology & Oceanography*, *32*(2), 396–402. https://doi.org/10.4319/lo.1987.32.2.0396

Schultz, M. G., Diehl, T., Brasseur, G. P., & Zittel, W. (2003). Air pollution and climate-forcing impacts of a global hydrogen economy. *Science*, *302*(5645), 624–627. https://doi.org/10.1126/science.1089527

Scranton, M. I. (1984). Hydrogen cycling in the waters near Bermuda: The role of the nitrogen fixer, oscillatoria thiebautii. *Deep-Sea Research, Part A: Oceanographic Research Papers*, *31*(2), 133–143. https://doi.org/10.1016/0198-0149(84)90020-7

Sengupta, D., Bharath Raj, G. N., & Shenoi, S. S. C. (2006). Surface freshwater from Bay of Bengal runoff and Indonesian throughflow in the tropical Indian Ocean. *Geophysical Research Letters*, *33*(22), L22609. https://doi.org/10.1029/2006GL027573

Shao, Z., Xu, Y., Wang, H., Luo, W., Wang, L., Huang, Y., et al. (2023). Global oceanic diazotroph database version 2 and elevated estimate of global oceanic N_2 fixation. *Earth System Science Data*, *15*(8), 3673–3709. https://doi.org/10.5194/essd-15-3673-2023

Shetye, S. R., Shenoi, S. S. C., Gouveia, A. D., Michael, G. S., Sundar, D., & Nampoothiri, G. (1991). Wind-driven coastal upwelling along the western boundary of the Bay of Bengal during the southwest monsoon. *Continental Shelf Research*, *11*(11), 1397–1408. https://doi.org/10.1016/0278-4343(91)90042-5

Shiozaki, T., Furuya, K., Kodama, T., Kitajima, S., Takeda, S., Takemura, T., & Kanda, J. (2010). New estimation of N_2 fixation in the western and central Pacific Ocean and its marginal seas. *Global Biogeochemical Cycles*, *24*(1), 1–12. https://doi.org/10.1029/2009GB003620

Warwick, N. J., Bekki, S., Nisbet, E. G., & Pyle, J. A. (2004). Impact of a hydrogen economy on the stratosphere and troposphere studied in a 2-D model. *Geophysical Research Letters*, *31*(5), 2–5. https://doi.org/10.1029/2003gl019224

Wei, W., Zhang, Y. T., Wang, C., Guo, W., Ngo, H. H., Chen, X., & Ni, B. J. (2022). Responses of anaerobic hydrogen-producing granules to acute microplastics exposure during biological hydrogen production from wastewater. *Water Research*, *220*, 118680. https://doi.org/10.1016/j.watres.2022.118680

Xiao, X., Prim, R. G., Simmonds, P. G., Steele, L. P., Novelli, P. C., Huang, J., et al. (2007). Optimal estimation of the soil uptake rate of molecular hydrogen from the Advanced Global Atmospheric Gases Experiment and other measurements. *Journal of Geophysical Research*, *112*(7), 1–15. https://doi.org/10.1029/2006JD007241

Xie, H., Andrews, S. S., Martin, W. R., Miller, J., Ziolkowski, L., Taylor, C. D., & Zafiriou, O. C. (2002). Validated methods for sampling and headspace analysis of carbon monoxide in seawater. *Marine Chemistry*, *77*(2–3), 93–108. https://doi.org/10.1016/S0304-4203(01)00065-2

References From the Supporting Information

Jähne, B., Heinz, G., & Dietrich, W. (1987). Measurement of the diffusion coefficients of sparingly soluble gases in water. *Journal of Geophysical Research*, *92*(C10), 10767–10776. https://doi.org/10.1029/JC092iC10p10767

Wanninkhof, R. (1992). Relationship between wind speed and gas exchange over the ocean. *Journal of Geophysical Research*, *97*(C5), 7373–7382. https://doi.org/10.1029/92JC00188

Wiesenburg, D. A., & Guinasso, N. L. (1979). Equilibrium solubilities of methane, carbon monoxide, and hydrogen in water and sea water. *Journal of Chemical and Engineering Data*, *24*(4), 356–360. https://doi.org/10.1021/je60083a006